

Grant Brandal¹

Mechanical Engineering Department,
Columbia University,
500 W 120th Street, Mudd Rm 220,
New York, NY 10023
e-mail: gbb2114@columbia.edu

Y. Lawrence Yao

Fellow ASME
Columbia University,
New York, NY 10023
e-mail: yly1@columbia.edu

Syed Naveed

Endoscopy Division,
Boston Scientific Corporation,
Marlborough, MA 01752
e-mail: Syed.naveed@bsci.com

Biocompatibility and Corrosion Response of Laser Joined NiTi to Stainless Steel Wires

The biocompatibility of nickel titanium (NiTi) wires joined to stainless steel (SS) wires via laser autogenous brazing has been evaluated. The laser joining process is designed to limit the amount of mixing of the materials, thus preventing the formation of brittle intermetallic phases. This process has the potential for manufacturing implantable medical devices; therefore, the biocompatibility must be determined. Laser joined samples underwent nickel release rate, polarization, hemolysis, and cytotoxicity testing. Competing effects regarding grain refinement and galvanic effects were found to influence the corrosion response. After 15 days of exposure to a simulated body fluid, the total nickel released is less than 2 ug/cm^2 . Numerical modeling of the corrosion currents along the wires, by making use of polarization data, helped to explain these results. Microbiological testing found a maximum hemolytic index of 1.8, while cytotoxicity tests found a zero toxicity grade. All of these results indicate that the autogenous laser brazing process results in joints with good biocompatibility. [DOI: 10.1115/1.4029766]

Introduction

Nickel titanium (NiTi) is a special material in that it is a shape memory alloy and exhibits superelasticity. For shape memory, after the material has been deformed, heating above a threshold temperature will cause the NiTi to return to its original shape. Superelasticity is the capability of the material to withstand large amounts of strain, via a diffusionless phase transformation.

These two properties have been found to be especially useful for developing medical devices. For example, a stent made of NiTi can be compressed to fit inside a catheter, moved into the desired position in the body, and then upon removal of the catheter the NiTi will spring back into its original shape because of its superelasticity. NiTi can also be used for bone staples and Simon vena cava vein filters [1]. The shape memory effect can be exploited by positioning the NiTi as an actuator on the end of a wire, acting as scissors or graspers. In this type of setup, the NiTi must be joined to a second material, to act as a foundation for movement. SS is a common material to pair with nickel titanium. Joining can be accomplished via adhesives, mechanical joints, or thermal processes such as welding or brazing. Cost reduction can also be achieved by joining dissimilar materials.

For implantable medical devices, mechanical joints are too bulky, and adhesives will not last in the corrosive environment of the body. Thermal joining processes often end up being the preferred method. But electric spot welding of NiTi to NiTi has been shown to significantly increase cytotoxicity [2]. Safer joining methods must be established. Further complicating things, metallurgical issues arise when NiTi and SS are joined. The phases formed by mixtures of these two materials are brittle intermetallics [3]. Since one of the main reasons for using NiTi is its flexibility, brittle joints are inadequate. Utilizing laser joining technology is a common way to make effective NiTi-SS joints, as will be described later. Since these joints are being placed in the body, it is important to ensure that they possess good biocompatibility. Numerous studies determining the biocompatibility of the base

nickel titanium and SS materials have been reported [4–6]. In general, both of these materials are considered as biocompatible.

Most of the proposed methods of laser joining NiTi to SS require using an interlayer of a third material, which suppresses brittle intermetallics formation. The corrosion response of samples using a copper interlayer was reported by Zhang et al. [7]. Commonly, nickel is used as an interlayer as well. This can give good mechanical strength [8], but introducing a third material (especially pure Ni) is undesirable because it will add more biocompatibility concerns. If the polarization response of the interlayer is more active than the other materials, galvanic concerns will be greatly enhanced from surface area considerations. Investigations of the biocompatibility of NiTi laser joined directly to SS to date have not been reported. Previous publications by the authors described a process to increase the tensile fracture strength of laser joined NiTi-SS joints [9,10] without the use of an interlayer, and is referred to as “autogenous laser brazing.” Now, this paper will explore the biocompatibility and corrosion response of this type of joint. Investigations into the nickel release rate, cytotoxicity, hemolytic response, and corrosion morphology are made.

Background

Laser Autogenous Brazing. Nickel titanium is nearly equiatomic, and iron is the most prevalent element in SS. A Ti-Ni-Fe ternary phase diagram can thus be used to determine which phases are formed when these three elements are melted and brought into contact with each other [11]. All of the potential phases that form (NiTi₂, FeTi, Fe₂Ti, and Ni₃Ti) are brittle intermetallics. Excessive amounts of these brittle phases will decrease the fracture strength of the weld. Using lasers as the input heat source can help to limit the formation of these phases by preventing overmelting. Figure 1 shows a schematic diagram of the autogenous laser brazing setup. The laser starts a fixed distance away and is scanned at a constant velocity toward the interface. Simultaneously, the wires are rotated, to ensure radially uniform heating. Thermal accumulation occurs at the interface since there is a thermal resistance between the two wires. The thermal accumulation results in a high localization of heating, so that only a very limited amount of the NiTi will melt and then wet onto the SS wire. Thus, a narrower region of intermetallics forms, resulting in increased fracture strengths. For additional strength, the wires have been

¹Corresponding author.

Contributed by the Manufacturing Engineering Division of ASME for publication in the JOURNAL OF MANUFACTURING SCIENCE AND ENGINEERING. Manuscript received May 6, 2014; final manuscript received January 20, 2015; published online March 5, 2015. Assoc. Editor: Wei Li.

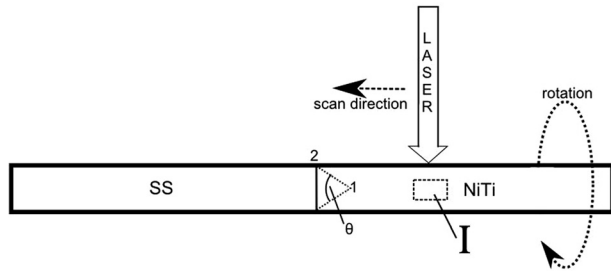


Fig. 1 Schematic diagram illustrating the autogenous laser brazing setup. The wires are rotated, while the laser simultaneously scans toward the interface, but is turned off before crossing over to the SS side. The angle θ corresponds to the apex angle of the cup/cone configuration.

fashioned into a cup and cone geometry, which provides mechanical benefits [9].

Biocompatibility Concerns. Biocompatibility refers to the ability of a material to be in contact with the human body without having any harmful or toxic effects. For implantable devices, it is important that the materials do not release excessive amounts of toxic elements via corrosion. Factors such as the corrosive products, environment, and duration of exposure all play a role in a material's biocompatibility. As such, there are not absolute thresholds as to whether a material is considered biocompatible or not. For example, the amount of nickel released from NiTi exposed to saliva is dependent on the fluoride and chloride concentrations in the saliva [12]. A device safe for use in the mouth may not be safe for exposure to blood. Temperature also plays a significant role in corrosion. Pitting of NiTi occurs most easily when the saliva temperature is in between the austenite start and finish temperatures [13]. During wound healing, blood becomes much more oxidizing [14], resulting in varying corrosion of the NiTi. The dynamic nature of the body makes it difficult to set absolute thresholds, and as such, the specific applications must be accounted for when determining the biocompatibility of a material.

In the material pair we are working with, NiTi is of the most concern, as it is composed of nearly 50% nickel. The human body is allergic to very small nickel concentrations, with some people being hypersensitive. Even though some small amounts of nickel are necessary for nutrition and healthy metabolism, direct release of nickel into the body from an implanted device is of great concern. The amount of nickel present in foods that actually gets absorbed by the body is in the range of 1–20% [15]. Subsequently, devices that are implanted directly into the bloodstream, such as stents, must be scrutinized even more closely than those for oral applications. Blood platelets may become activated when contacted by nickel, causing thrombus formation in the blood stream [16]. Nickel also may activate monocytes, a type of white blood cell, which will lead to inflammation [17].

Despite its high nickel concentration, NiTi is generally considered biocompatible because it forms a passive titanium oxide layer on its entire outer surface. As a result, the high nickel concentration is not too detrimental to the biocompatibility of NiTi. Oxide layer depth is limited by the distance that electrons from the metal can tunnel through the oxide layer to reach the electrolyte solution [18]. Michiardi et al. found optimal parameters for thermal treating NiTi, and achieved an oxide layer that was 63 μm thick, approximately ten times thicker than the oxide of a mechanically polished sample [19]. Plasma source ion implantation can be used to introduce additional oxygen, increasing the corrosion resistance of NiTi [20]. Uniformity of this layer plays an important role, and as such, any regions where the oxide layer is damaged or thinned will be detrimental [21].

The oxide layer formed on NiTi is capable of withstanding large deformations [22]. This allows for the superelasticity of

NiTi to be used in medical devices. Since implementations of NiTi usually involve high levels of strain, having an oxide layer sensitive to deformation would make NiTi much less useful, as oxide layer breakdown would lead to increased nickel release. NiTi's oxide layer has several different compositions in the depth profile, and the order and depth of these layers is dependent on the previous surface treatments [23]. This varying depth profile will cause the nickel release rate to go through several different stages with respect to time. Armitage et al. found the biocompatibility of NiTi to be similar to that of pure titanium [16], but some nickel is still released. SS is composed of 8–11% nickel. When exposed to a simulated body fluid, it has a nickel release rate of less than $0.03 \mu\text{g cm}^{-2} \text{ week}^{-1}$, which is a safe level. Similar to NiTi, the biocompatibility is the result of the formation of a passive oxide layer. In this case, it is a passive chromium oxide layer that protects the nickel from being released.

Divergence From Base Material Response. Even though both NiTi and SS are initially considered to be safe, their biocompatibility may be decreased from thermal effects of the joining process. Elevated temperatures altering the grain size and oxide layer will result in a varied corrosion response. The melting temperature of NiTi is slightly lower than that of SS. Since we are hoping to only melt one material using laser autogenous brazing, we irradiate the NiTi during the laser scan. This way we can ideally keep the entire part below the SS's melting temperature during processing. The result on biocompatibility is that most of the laser modification of material properties is limited to the nickel titanium. Several different methods of using laser surface treatments to increase NiTi's corrosion behavior have been reported. Villermaux et al. used excimer laser treatment to thicken the oxide layer and increase uniformity, effectively increasing the biocompatibility of NiTi [24]. But in our case, the laser treatment has been set to maximize the fracture strength of the joint, rather than to optimize oxide layer growth. As the NiTi is heated, TiNi_3 may precipitate out at the grain boundaries [25]. A homogeneous passive oxide layer will not form across multiphase surfaces, and the corrosion resistance will therefore be decreased if excessive TiNi_3 is formed [26].

Polarization Tests. When placed in an electrolyte, a material will have an equilibrium electric potential that it will naturally reach. Any deviation from this potential will cause changes in the corrosion current from the material. This current is electrons that are released from the surface, and for NiTi, accompanying Ni^+ ions will also be introduced to the body. The response a material has to deviations from its equilibrium potential is described by the Butler–Volmer equation [27]

$$i = i_o e^{\left(\frac{\alpha n F}{RT} \eta\right)} - i_o e^{\left(-\frac{(1-\alpha) n F}{RT} \eta\right)} \quad (1)$$

where i is the current density, α is the charge transfer coefficient, n is the number of electrons for the reaction, R is the gas constant, T is temperature, and η is the overpotential (difference from equilibrium). When the material is held at a potential much greater than its equilibrium, η becomes large in the positive direction, and the first exponential term will dominate, and vice versa for negative values of η . In these limits, Eq. (1) can be rearranged to give the Tafel Equations as [28]

$$\eta_c = \beta_c \log\left(\frac{i_c}{i_o}\right) \quad (2)$$

$$\eta_a = \beta_a \log\left(\frac{a}{i_o}\right) \quad (3)$$

where c and a represent the cathode and the anode, and β accounts for the activation polarization.

Joining dissimilar metals results in a galvanic couple, in which one of the metals is preferentially corroded. Plotting the polarization curves of the materials on the same graph can predict how large the galvanic corrosive effect will be, where the corrosion potential and current for the joined part will be the point on the graph where the polarization curves intersect.

Mixed potential theory, as described above, is a method to roughly estimate the corrosion current of a joined sample. But, it is restrictive in that it does not take into account the geometrical features and spatial distribution of the part. The regions far from the dissimilar interface will have the same behavior as the base material response, indicating the corrosion current will decay as we move toward the outer regions. A way to determine the anisotropy of current along the part is by calculating the Wagner parameter. The Wagner parameter is defined as [29]

$$W = \left[\rho \frac{di}{dE} \right]^{-1} = \sigma R_p \quad (4)$$

where ρ and σ are the resistivity and conductivity of the solution, respectively, di/dE is the slope from the polarization curve, and R_p is the polarization resistance. Physically, the Wagner parameter is the ratio of the resistance of the metal over the resistance of the electrolyte. As this number gets large, the spatial distribution of current will become more uniform along the metal, and vice versa.

Numerical Modeling. A finite element model was created to determine the spatial distribution of the current on a joined wire sample. The governing equation for this situation is the Nernst–Planck equation, which describes ion flow in a fluid. This is given as

$$\frac{\partial c_n}{\partial t} = \nabla \cdot \left[D_n \nabla c_n - u_n c_n + \frac{D_n Z_n e}{K_B T} c_n \left(\nabla \phi + \frac{\partial \hat{A}}{\partial t} \right) \right] \quad (5)$$

where n represents the species, c is concentration, D is the diffusivity of chemical species, u is the velocity of the fluid, Z is the valence of the ion, e is the electron charge, K_B is Boltzmann’s constant, T is temperature, ϕ is the electric potential, and \hat{A} is the magnetic vector potential. For application to our joined wires, the Nernst–Planck equation is solved in the electrolyte, and the wires get included as boundary conditions. This setup is illustrated in Fig. 2. Azimuthal symmetry of the wires makes it possible to

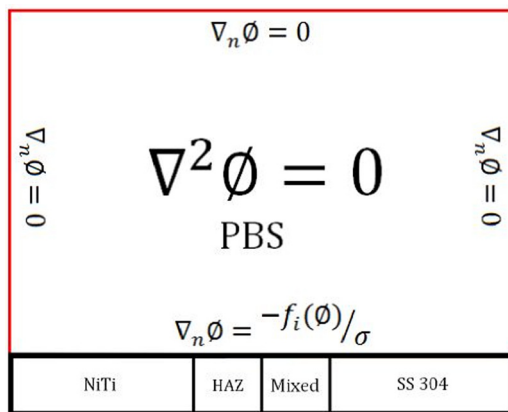


Fig. 2 Visual description of the numerical model used for prediction of the galvanic current. Laplace’s equation is solved in the electrolyte PBS. Material properties are taken into account as the relevant boundary conditions along the bottom border. The function $f_i(\phi)$ is the polarization response for the respective material.

model this using only two-dimensional. We assume there is no magnetic field present and that the electrolyte is stationary, electroneutral, and well-mixed. The well-mixed electrolyte leads to having no concentration gradient, i.e., $\nabla c_n = 0$. These simplifications reduce Eq. (5) to Laplace’s equation

$$\nabla^2 \phi = 0 \quad (6)$$

Using the results of the polarization tests now allows for inclusion of the SS and NiTi material properties. Let $I_{NiTi}(\phi)$ and $I_{SS}(\phi)$ be the respective polarization curves. Dividing these by the conductivity of the electrolyte, σ , gives the Neumann boundary conditions as [30]

$$\nabla \phi = \frac{-I(\phi)}{\sigma} \quad (7)$$

The laser irradiated region and the actual joint do not contain enough surface area to explicitly measure the polarization response by traditional methods. But it is known that the polarization response of the mixed region of the joint lies in between the responses of the base materials [31]. Therefore, $I_{NiTi}(\phi)$ and $I_{SS}(\phi)$ were averaged to produce $I_{mixed}(\phi)$. In addition, a fourth region simulating the heat affected zone (HAZ) of the NiTi was also used. The equilibrium potential of laser surface treated NiTi lies slightly more noble than that of the base NiTi [32]. Shifting the NiTi curve gives us the response of the HAZ of NiTi. This setup was solved using COMSOL.

Microbiology Testing. Electrochemical techniques that determine the rate of corrosion are an indirect way of determining biocompatibility, since assumptions on the effect of the ions released from corrosion must be made. A direct approach is to do hemolysis and cytotoxicity testing. These are both microbiological tests that measure the interaction of the sample with various biological cells. Oftentimes implantable medical devices will be exposed directly to blood, as would be the case for a stent. The amount of red blood cells destroyed from contact with the sample is determined via hemolysis testing. Samples are exposed to a serum for 72 hr, and then brought into contact with rabbit blood samples. When red blood cells are destroyed, they release hemoglobin, and the hemoglobin concentration is measured using a spectrophotometer [33]. The percentage of cells destroyed gets reported as the hemolytic index, where indexes ranging from 0 to 2 are considered to be safe, while anything above five is considered as hemolytic and nonbiocompatible.

Similarly, cytotoxicity tests are used to measure cell death. The wire samples are exposed to a serum, and then this serum is extracted and placed into contact with a cell culture obtained from mice. On a scale of zero to four, the amount of cell destruction is qualitatively determined as either nontoxic or toxic [34].

Experimental Procedure

Nickel titanium and SS 304 wires with 762 μm diameters were used. The composition of the NiTi is 54 at. % Ti and 46 at. % Ni, with the austenitic finish temperature below room temperature. A conical apex angle of 90 deg was used for all the joints. Rotation of 5000 rpm against 320 grit silicon carbide abrasive paper formed the cones on the end of the SS wires. The nickel titanium wires were first flattened on the ends using the same type of abrasive paper. Then, a 1143 μm diameter spot drill was used to form the cup-like shape. Laser joining was achieved via an SPI redENERGY G4 fiber laser, with a wavelength of 1064 nm and operating in continuous wave mode. Laser powers ranging from 13–17 W were used, and the rotation speeds ranged from 1500 deg/s to 3000 deg/s. The laser started 1.6 mm away from the interface, on the NiTi side, and then scanned toward the interface at a linear velocity, stopping 0.1 mm before it reached the SS.

Phosphate buffered saline (PBS) was used as the electrolyte for the corrosion tests. As the end product is implantable medical devices, the PBS acted as a simulated body fluid to mimic the environment of the body. The PBS was 1X concentration, whose components are 0.138 M NaCl and 0.0027 M KCl. The polarization responses of the nickel titanium and SS were obtained following the methods of ASTM G5 [35]. All potentials are with respect to a saturated calomel electrode. Degradation testing was performed in vials containing 22 ml of PBS at 37°C. Laser power was 17 W, and this time rotational speeds of 1500 deg/s and 2500 deg/s were analyzed. Three wire joints were placed in each vial, and five duplicate vials were made. Joints were removed in progressive intervals, at 1, 3, 6, 10, and 15 days. The leftover fluid, with corroded materials, was used for nickel concentration analysis via inductively coupled plasma atomic emission spectroscopy, following protocol of EPA 200.7 Rv. 4.4 [36]. Imaging of the corroded wires was carried out on a Hitachi-S47 00 SEM. Grain size and phase determination was achieved using electron backscatter diffraction (EBSD). For the microbiology tests of hemolysis and cytotoxicity, ASTM756 and ISO 10993-5 were used, respectively. Cell line L929 was implemented for the cytotoxicity tests.

Results

Polarization Tests. The results of the polarization tests are presented in Fig. 3, where the solid lines are measured quantities and the dotted lines represent estimations. Since the equilibrium potential of NiTi is lower than that of SS, it is clear that the NiTi will act as the anode for the galvanic couple, resulting in more nickel ions being released into the electrolyte. Mixed potential theory suggests that the corrosion of the joined wires will increase by at least a factor of ten compared to the base materials. When the potential of the SS rises above 0.2 V, the oxide layer breaks down, and the corrosion current rapidly increases. The breakdown potential of NiTi is not shown on the plot, but at some higher potential it would have similar behavior. The polarization resistance for each material is extracted from Fig. 3, and plugged into Eq. (5) to determine the respective Wagner parameters. PBS has a conductivity of 15,000 $\mu\text{mhos/cm}$. This results in $W_{\text{NiTi}} = 43.5 \text{ m}$ and $W_{\text{stainless}} = 22.5 \text{ m}$. Both of these numbers are rather large, suggesting a somewhat uniform current distribution. Although the

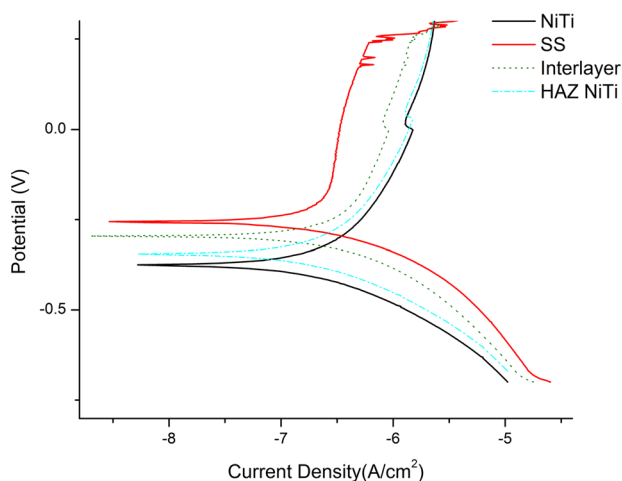


Fig. 3 Polarization response of metal samples in PBS solution. The solid lines indicate measurements, while the dashed lines are approximations. The more electronegative equilibrium potential of the NiTi will cause it to experience anodic effects, while the SS is cathodic. When the transition from the base materials goes through the two intermediary phases, the corrosion current gets significantly reduced. This data was used for $f(\phi)$ in Fig. 2.

stainless will have a slightly less uniform response traveling away from the interface.

Corrosion Current Modeling. The electric potential of the PBS electrolyte is plotted in Fig. 4, with the arrows indicating the gradient of this field, representative of the direction of current flow. Using the results from the polarization tests, the spatial distribution of the electron current density was determined across the wires. This distribution is displayed in Fig. 5. The solid lines are the currents for corrosion in PBS, while the dotted lines are for comparison to the corrosion response in an electrolyte with 1/10 the conductivity of PBS. Blood has a very similar nominal conductivity to that of PBS. But, the orientation of the erythrocytes will greatly impact the conductivity. This orientation could be dependent on whether the blood is flowing or stationary. Blood flowing at high velocity can have a conductivity as low as 1/10 that of stationary blood [37], corresponding to the dashed lines in Fig. 5. Regions with positive values of electron flow are anodic, that is, these are the regions attacked by the galvanic couple, while the regions with negative current density are not releasing ions into the electrolyte and therefore are being galvanically protected. Both of the intermediary regions have lengths of 1 mm, corresponding to length of the laser interaction.

As is predicted by Wagner parameter analysis, lowering the conductivity of the electrolyte results in a more nonuniform distribution of current density. On the NiTi, the current adjacent to the HAZ is nearly 50% larger than that toward the end of the wire. Since it has a smaller polarization resistance, the SS is even more nonuniform, with the current across the segment varying by almost 100%.

Current densities for the PBS simulated model are more uniform, again consistent with the Wagner parameter. We see that the stainless has more nonuniformity than the NiTi though. The NiTi lies slightly above $3 \times 10^{-7} \text{ A/cm}^2$, which is a rather low current. This is desirable, and suggests that this galvanic pair is likely to have good biocompatibility properties, since the amount of nickel released into the electrolyte is not going to be excessive. In a way, the HAZ NiTi and the mixed region act as stepping stones for the galvanic couple, effectively lowering the predicted current. Figure 3 suggests that if the NiTi was coupled directly to the SS, the corrosion current would be on the order of $10^{-6.5} \text{ A/cm}^2$, about 30% higher than the currents calculated using the numeric model. In reality, the transition from the base NiTi to the

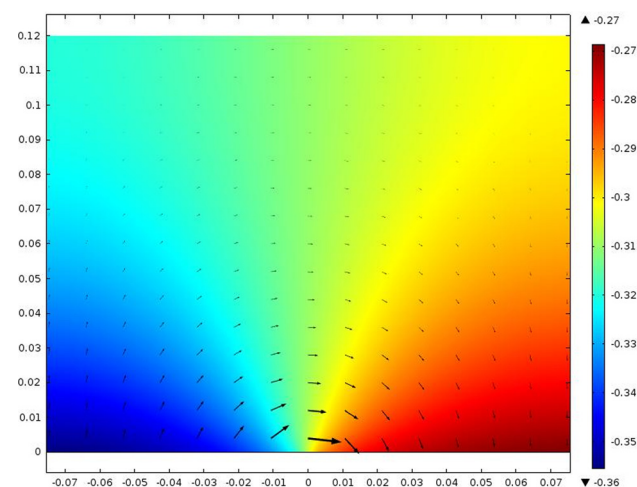


Fig. 4 Numerical simulation results for the distribution of the electric potential in the PBS solution. The gradient of this field gives the direction of electron flow and is denoted via the arrows. At either extreme along the bottom boundary, the potential approaches the equilibrium potential of the respective material nearby.

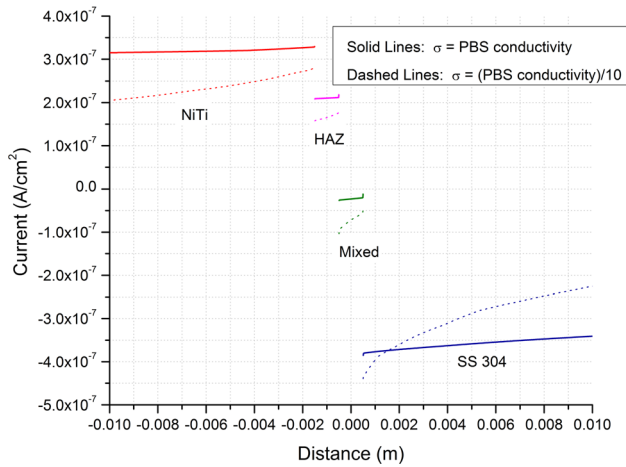


Fig. 5 Distribution of electron flow along the lower boundary of Fig. 4, corresponding to the corrosion current. The dotted lines are for a electrolytic conductivity that is only 10% that of the solid lines, causing a more nonuniform distribution.

HAZ is continuous (corresponding to the temperature gradient formed from thermal accumulation), rather than the step function that was defined in the model. But, since we are unable to measure this transition using potentiostat testing, the simplified configuration was used.

Nickel Release Tests. For reasons previously described, the release of nickel from corroding NiTi is of the most concern. Titanium ions will be released as well, but these are of much less biological concern, and the relative quantity of titanium released is known to be much less than that of nickel [38]. As such, the release of nickel will be our focus. Plots of the nickel release as a function of exposure time in the PBS are presented in Fig. 6. While both of the parameters investigated release similar amounts of nickel, it is of interest to note that in some places the sample that was processed with a lower thermal input actually releases more nickel. At first, this may seem counterintuitive, but several physical phenomenon may help to describe why this is so, as will be described in the following section discussing thermally induced changes.

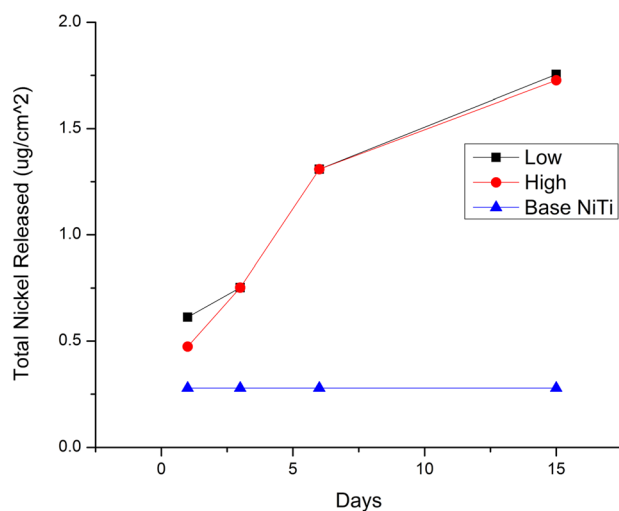


Fig. 6 Total amount of nickel released from joined samples as a function of time. The two different processing parameters of low and high energy inputs have similar profiles, but are noticeably higher than the base NiTi. This NiTi has undergone a previous heat treatment; nontreated NiTi has a release profile higher than the treated samples in here in our case.

The most important characteristic is that both of the processed samples release significantly higher amounts of nickel than the base NiTi does. Before the laser joining process, the NiTi has previously undergone a thermal treatment to optimize the oxide layer so that minimal nickel is released. In comparison to other reported nickel release rates, it is noted that even our joined samples release less nickel than most untreated NiTi does [4], showing that laser autogenous brazing conserves the biocompatibility of the base materials.

Morphology and Thermally Induced Changes. The regions where the galvanic current is the highest and where the NiTi is directly irradiated overlap with each other, resulting in competing effects in terms of influencing the corrosion current and nickel ion release. Overmelting results in a larger mixed and deformed region at the interface, which will not have a uniform oxide layer, and is seen in Figs. 7 and 8. Surface roughness and cracks in this region also are more susceptible to crevice corrosion, suggesting higher processing powers will increase the amount of corrosion. This is illustrated in Fig. 9, which shows images of the surface in this deformed region after 6 and 15 days of corroding.

An optical micrograph of a longitudinally sectioned joint is presented in Fig. 10. Only the bottom half of the wires is represented, as the top half is symmetric. Many different regions are seen on the nickel titanium side. Colloidal silica was used in the final polishing step for this sample, which acts as a mild etchant to help identify grain distribution and size. The grains nearest to the interface are the largest, which can be attributed to the thermal accumulation occurring in this region. As discussed by Satoh [39], the grain size will gradually decrease as we move away from the interface. In the nonHAZ regions of the NiTi, the grains are too small to see using optical microscopy. Electron microscopy can be used to increase the resolution and magnification. Figure 11 is an EBSD map illustrating the grain size and distribution of the NiTi in a region further removed from the interface. Each color represents a unique grain. Many of these grains have diameters less than 200 nm. Pretreating the material and cold-working is used to refine the grain size to this small value, as described by Crone [40], which is done for mechanical property considerations. The corrosion current will increase as the grain size is decreased, which can be expressed as [41]

$$i_{\text{corrosion}} = A + \frac{B}{\sqrt{\text{grain size}}} \quad (8)$$

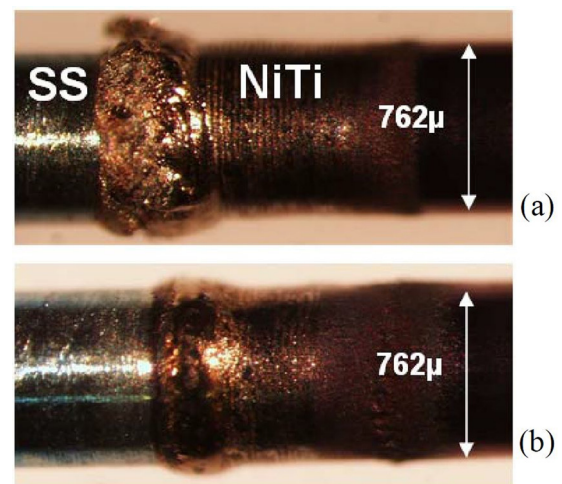


Fig. 7 Optical images comparing the interface regions for two different laser power levels. Both underwent a rotational speed of 3000 deg/s, (a) had a laser power of 15 W while (b) was irradiated at 13 W. The HAZ of the NiTi progresses through several regions before the material starts to bow out at the interface.

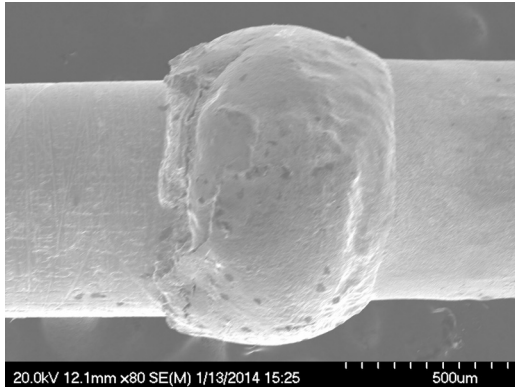


Fig. 8 SEM image of the outside interface for a joined sample. Roughness and nonuniformity is evident in this region, making it susceptible to effects such as pitting and crevice corrosion.

where both A and B are material constants. This relationship arises from the fact that grain boundaries are weaker, and more susceptible to releasing ions into the electrolyte. Higher temperatures reached during processing will result in larger grains being formed. Thus from a grain size argument, wires processed with higher laser input will have lower corrosion currents. Amorphous NiTi is even more corrosion resistant and has a higher pitting potential, because it lacks grain boundaries [42]. But, amorphous NiTi is much harder and is difficult to shape or machine into complex parts.

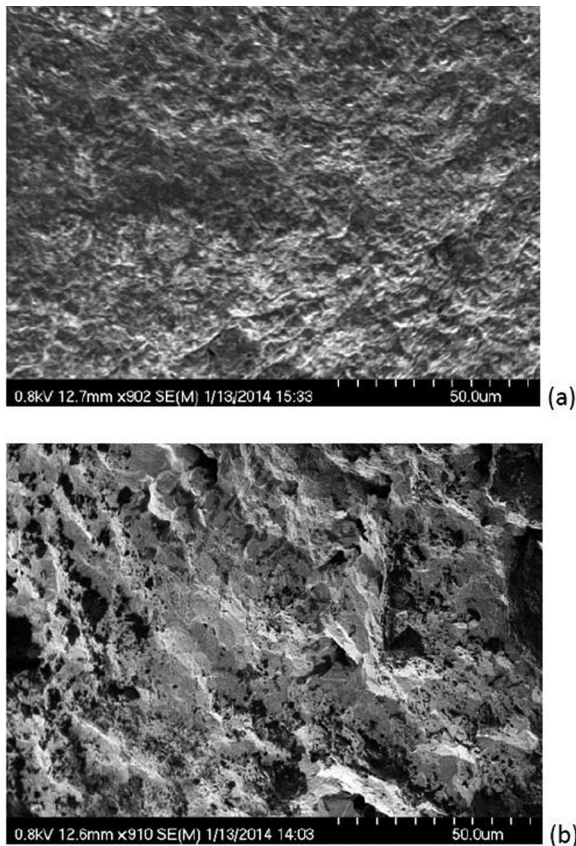


Fig. 9 Surface corrosion at the mixed interface region after 6 days (a) and 15 days (b) of exposure to the simulated body fluid. Both samples were joined at 17 W and 1500 deg/s. Rather uniform texture is seen in (a), but this surface becomes much rougher as corrosion proceeds, as evidenced by the sharper regions found in (b).

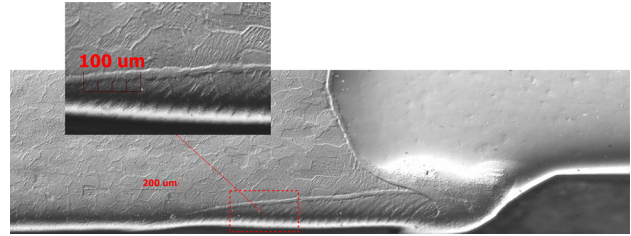


Fig. 10 Optical micrograph at the interface of a longitudinally sectioned sample. Distinct grains are clearly visible in the NiTi on the left hand side, with size increasing nearer to the interface. The inset shows an enlarged image near the outer edge, where the combination of stress and elevated temperatures resulted in dynamic recrystallization. This is a region that recrystallized without having reached the melting temperature.

This phenomenon means that we will have competing effects for the corrosion current that flows. The effect of the galvanic couple is that the corrosion current near the interface will be increased, but the larger grains in this region will try to resist this increase in corrosion. The gradual, continuous increase of grain size near the interface suggests that melting of the NiTi has not occurred. Grain growth in the solid state occurs when atoms in the grain boundary attach onto an adjacent grain, in order to decrease the grain boundary energy. Any melting would have been accompanied by a region that has smaller grains, which had been quenched by the cooler SS side. The inset of Fig. 10 shows a larger version of the peculiar refined region found near the outside of the NiTi. This line is composed of a string of smaller sized grains, while the grains above and below it have similar sizes to the bulk of the material. This cannot simply be a melted region, since the grains at the outside of the wire (which underwent direct laser irradiation) would also have to be smaller in this case. Instead, dynamic recrystallization may be occurring in this region. Dynamic recrystallization is a phenomenon whereby the combination of stress and elevated temperatures can nucleate new grains [43]. In NiTi this can occur 1073–1273 K [43], well below the NiTi melting temperature of 1583 K. As can be seen in Fig. 10, the recrystallized region is aligned with the outside edge of the SS wire, which may account for a localized stress concentration, sufficient for dynamic recrystallization.

On the right hand side of Fig. 10 is the SS, which has a rather uniform morphology. That is, the thermal input from the laser appears to change very little of the structure. Since the laser never

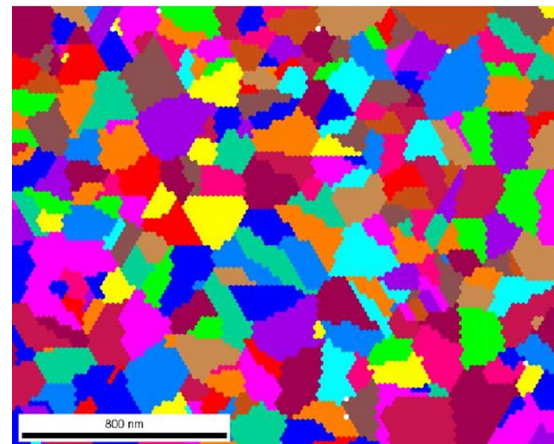


Fig. 11 EBSD unique grain map in a region of NiTi far from the interface. The rather small grain size may be an effect of previous cold-working. When compared with the sizes of Fig. 10, it is clear that the thermal accumulation of the interface results in significant grain growth.

directly irradiates the SS side, it is clear that minimal HAZs should be present in the SS. Even if the laser happened to cross over the interface, it would not be much of a concern for the corrosion response of the SS since it is known that laser surface melting of SS helps to increase its corrosion resistance [44]. But the reason that irradiation of the SS is avoided is that keeping the SS below its melting temperature prevents mixing and brittle intermetallic formation, subsequently decreasing the mechanical strength of the joint. The region near the interface along the bottom appears to have melted and resolidified into a smaller grain structure.

Grain growth is not the only thermal effect that could occur in the materials. Elevated temperatures may result in some of the materials' components precipitating out, and thus altering the corrosion behavior. In SSs, chromium is insoluble in iron from 425 °C to 815 °C, so chromium carbide will precipitate out at the grain boundaries resulting in depleted regions [28]. These chromium depleted regions (along the grain boundaries) will be more susceptible to corrosion, with this process being referred to as "sensitization." Microgalvanic corrosion then occurs, because the regions with less chromium are more active in the electrolyte. Detection of this can be done via EBSD. Figure 12 shows an EBSD phase detection map in one of the most HAZs of the sample from Fig. 10. No chromium precipitates are detected. Multiple scans were performed across several different samples, and evidence of chromium precipitation was never detected. This suggests that the SS does not stay at the elevated temperature for a sufficient time for precipitation to occur, indicating again that the autogenous laser brazing process does indeed input only the minimum amount of energy necessary for joining. Similarly, the NiTi may undergo thermally induced precipitation as well. EBSD analysis was also performed on regions of the NiTi side, looking for precipitate formation, as seen in Fig. 11. But, no evidence of precipitates was seen in the NiTi either, which are beneficial for keeping the material properties of the processed wires as similar to those of the base material as possible. The small initial grain size may act as a barrier to precipitation forming, especially of Ni_4Ti_3 [45].

Even though no precipitates are formed in the HAZ of the NiTi wire, this region still has an altered corrosion response to the PBS electrolyte. Since the temperature distribution is very uniform in the axial direction, because of the high rotational velocity, the HAZ on the surface of the wires is essentially one-dimensional.

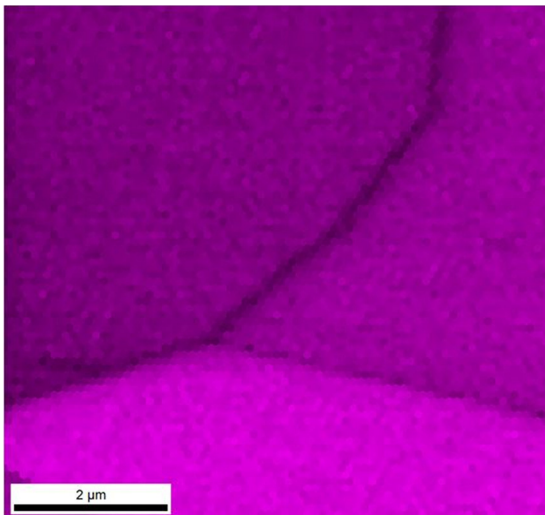


Fig. 12 EBSD phase map in a HAZ of the SS. At elevated temperatures, SS may become sensitized by precipitation of chromium along grain boundaries. This is a representative image of the whole region, and chromium precipitation was never detected. Thus, the biocompatibility of the SS is not harmed by the laser joining process.

SEM images of the border of the HAZ with the base material of two samples are presented in Fig. 13. Both of these samples underwent corrosion for 15 days, with (a) being processed with more laser energy than (b). It is clearly evident that the lower energy sample undergoes more corrosion in this case, which agrees with the results found via the nickel release tests. But, it is interesting to note that this occurs on both sides of the HAZ boundary. At higher heat inputs, the width of the mixed interface will become wider than that of lower powers. The presence of additional new material phases, such as TiFe_2 and TiFe , may act as electrical insulators. With respect to mixed potential theory, a resistance will shift the corrosion current to the left of the intersection in Fig. 3, effectively decreasing the amount of galvanic current that flows. Additionally, this could also be attributed to the larger grains in the more heated sample.

Cytotoxicity and Hemolysis. Two different processing parameters were tested for their biocompatibility using cytotoxicity and hemolysis testing. The largest difference in laser effects on the wires was desired, while still having joints that were mechanically strong. Both sets were rotated at 3000 deg/s during laser irradiation, but the power was 13 W for the low end and 17 W for the high.

For the cytotoxicity, both the low and high power samples returned toxicity grades of zero, indicating they are both nontoxic. At first this may seem unenlightening, but it does lead to an important realization. A window containing the processing parameters that result in good tensile strengths has been reported by the authors in a previous work [9]. The parameters used in these microbiology tests fall on the low and high ends of this window, indicating that the range of parameters useful for achieving high

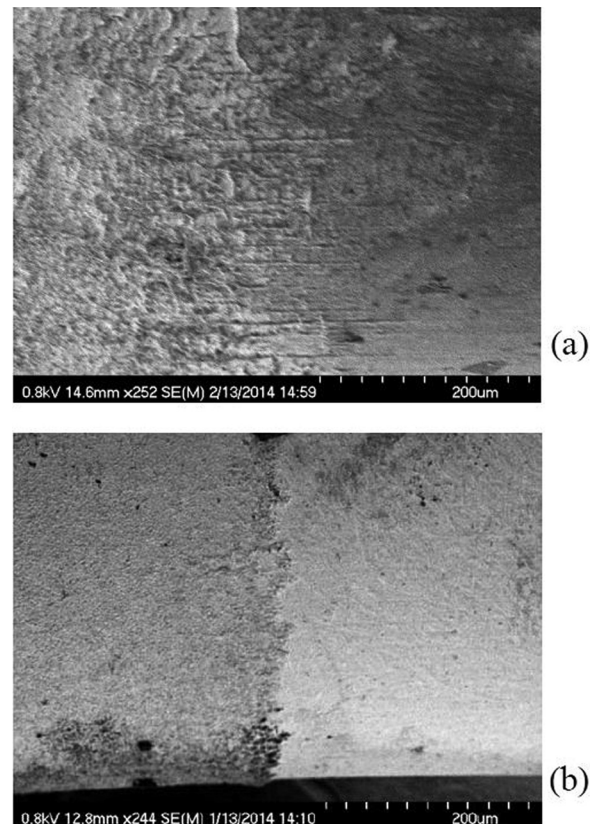


Fig. 13 Images of the border of the HAZ and base material in the NiTi, as indicated by the inset region of Fig. 1. More corrosion is evident in the lower power sample of (a) than for the higher power of (b). This is evidence that more intermetallic formation at the interface may act as an electrical resistance, effectively reducing the flow of the galvanic current.

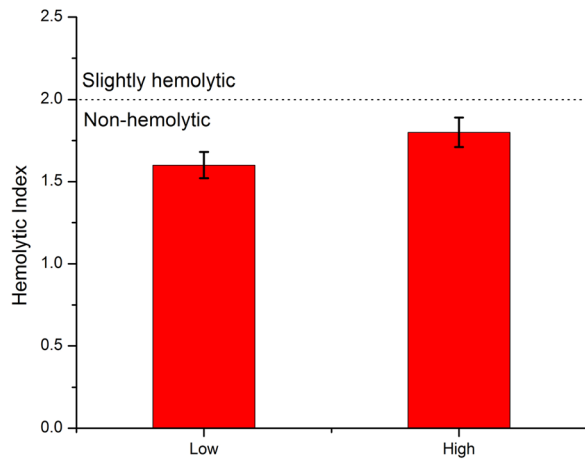


Fig. 14 Hemolysis testing for two different laser processing parameters. Slightly more hemolytic properties are found in the sample irradiated with higher energy, but both are well within the biocompatible, safe zone. Error bars indicate standard error.

strengths corresponds to a noncytotoxic range. If a significant trade-off between strength and biocompatibility was found, this would be detrimental to the applications of the autogenous laser brazing process.

Hemolysis testing is more sensitive than cytotoxicity and is capable of detecting differences between the samples' processing parameters. As seen in Fig. 14, samples irradiated at 13 W were found to have a hemolytic index of 1.6, while the samples irradiated at 17 W had a hemolytic index of 1.8. The standard error is 0.9, so the difference of the two parameters lies slightly outside of this uncertainty. Having a hemolytic index of less than two is considered to be nonhemolytic, so both of the parameters are within this safe zone. But the 17 W wires are approaching this upper limit. The base materials of unprocessed NiTi and SS are known to have hemolytic indexes in the range of 0.2–0.4 [16].

Conclusion

The range of processing parameters investigated here has been shown in a previous study by the authors to have drastic effects on mechanical strength [9]. But the biocompatibility across this range is found to be quite similar. This is beneficial for the application of autogenous laser brazing. If the parameters giving the strongest mechanical strength were different from those that provide good biocompatibility, implementation of the autogenous laser brazing process for manufacture of implantable medical devices would be restricted. We have found that many different factors influence the biocompatibility of the joined samples. Fortunately though, the differing effects appear to counter act with each other, and the end result is that the joined samples are slightly less biocompatible than unprocessed NiTi, but still lie within a safe range for implantation into the body.

Acknowledgment

This material was based upon work supported by the National Science Foundation under Grant No. CMMI-1130564. The authors also acknowledge financial support from Columbia University. Use of characterization equipment in the Shared Materials Characterization Laboratory, Columbia University, is also acknowledged. Thanks to Melissa Erickson for completing the microbiology testing.

References

- [1] Duerig, T., Pelton, A., and Stöckel, D., 1999, "An Overview of Nitinol Medical Applications," *Mater. Sci. Eng. A*, **A273**(275), pp. 149–160.

- [2] Dos Santos, R. L., Pithon, M. M., Nascimento, L. E. A. G., Martins, F. O., Teresa, M., Romanos, V., and Nojima, L. I., 2011, "Cytotoxicity of Electric Spot Welding: An In Vitro Study," *Dent. Press J. Orthod.*, **16**(3), pp. 1–6. Available at <http://dpjo.dentalpresspub.com/editions/v16n3/>
- [3] Vannod, J., 2011, *Laser Welding of Nickel-Titanium and Stainless Steel Wires: Processing, Metallurgy and Properties*, Ph.D. thesis, Ecole Polytechnique Federale De Lausanne, Lausanne, Switzerland.
- [4] Cui, Z. D., Man, H. C., and Yang, X. J., 2005, "The Corrosion and Nickel Release Behavior of Laser Surface-Melted NiTi Shape Memory Alloy in Hanks' Solution," *Surf. Coat. Technol.*, **192**(2–3), pp. 347–353.
- [5] Surmenev, R. A., Ryabtseva, M. A., Shesterikov, E. V., Pichugin, V. F., Peitsch, T., and Epple, M., 2010, "The Release of Nickel From Nickel-Titanium (NiTi) is Strongly Reduced by a Sub-Micrometer Thin Layer of Calcium Phosphate Deposited by RF-Magnetron Sputtering," *J. Mater. Sci. Mater. Med.*, **21**(4), pp. 1233–1239.
- [6] Hang, R., Ma, S., Ji, V., and Chu, P. K., 2010, "Corrosion Behavior of NiTi Alloy in Fetal Bovine Serum," *Electrochim. Acta*, **55**(20), pp. 5551–5560.
- [7] Zhang, C., Sun, X., Zhao, S., Yu, W., and Sun, D., 2014, "Susceptibility to Corrosion and In Vitro Biocompatibility of a Laser-Welded Composite Orthodontic Arch Wire," *Ann. Biomed. Eng.*, **42**(1), pp. 222–230.
- [8] Li, H. M., Sun, D. Q., Cai, X. L., Dong, P., and Wang, W. Q., 2012, "Laser Welding of TiNi Shape Memory Alloy and Stainless Steel Using Ni Interlayer," *Mater. Des.*, **39**, pp. 285–293.
- [9] Brandal, G., Satoh, G., Yao, Y. L., and Naveed, S., 2013, "Beneficial Interface Geometry for Laser Joining of NiTi to Stainless Steel Wires," *ASME J. Manuf. Sci. Eng.*, **135**(6), p. 061006.
- [10] Satoh, G., and Yao, Y. L., 2011, "Laser Autogenous Brazing—A New Method for Joining Dissimilar Metals," Proceedings of the 30th International Congress on the Applications of Lasers and Electro-Optics, Lake Buena Vista, FL, pp. 315–324.
- [11] Cacciamani, G., De Keyser, J., Ferro, R., Klotz, U. E., Lacaze, J., and Wollants, P., 2006, "Critical Evaluation of the Fe–Ni, Fe–Ti and Fe–Ni–Ti Alloy Systems," *Intermetallics*, **14**(10–11), pp. 1312–1325.
- [12] Li, X., Wang, J., Han, E., and Ke, W., 2007, "Influence of Fluoride and Chloride on Corrosion Behavior of NiTi Orthodontic Wires," *Acta Biomater.*, **3**(5), pp. 807–815.
- [13] Wang, J., Li, N., Han, E., and Ke, W., 2006, "Effect of pH, Temperature and Cl⁻ Concentration on Electrochemical Behavior of NiTi Shape Memory Alloy in Artificial Saliva," *J. Mater. Sci. Mater. Med.*, **17**(10), pp. 885–890.
- [14] Petro, R., and Schlesinger, M., 2013, *Applications of Electrochemistry in Medicine*, Springer, Boston, MA.
- [15] Expert Group on Vitamins and Minerals, 2003, "Safe Upper Levels for Vitamins and Minerals," Committee on Toxicity, Food Standards Agency, Report.
- [16] Armitage, D. A., Parker, T. L., and Grant, D. M., 2003, "Biocompatibility and Hemocompatibility of Surface-Modified NiTi Alloys," *J. Biomed. Mater. Res. A*, **66**(1), pp. 129–137.
- [17] Wataha, J. C., Lockwood, P. E., Marek, M., and Ghazi, M., 1999, "Ability of Ni-Containing Biomedical Alloys to Activate Monocytes and Endothelial Cells in Vitro," *J. Biomed. Mater. Res.*, **45**(3), pp. 251–257.
- [18] Fehlner, F., and Graham, M., 2002, "Thin Oxide Film Formation on Metals," *Corrosion Mechanisms in Theory and Practice*, P. Marcus, ed., Marcel Dekker, New York, pp. 171–187.
- [19] Michiardi, A., Aparicio, C., Planell, J. A., and Gil, F. J., 2006, "New Oxidation Treatment of NiTi Shape Memory Alloys to Obtain Ni-Free Surfaces and to Improve Biocompatibility," *J. Biomed. Mater. Res. B*, **77**(2), pp. 249–256.
- [20] Tan, L., 2003, "Corrosion and Wear-Corrosion Behavior of NiTi Modified by Plasma Source Ion Implantation," *Biomaterials*, **24**(22), pp. 3931–3939.
- [21] Trépanier, C., Tabrizian, M., Yahia, L. H., Bilodeau, L., and Piron, D. L., 1998, "Effect of Modification of Oxide Layer on NiTi Stent Corrosion Resistance," *J. Biomed. Mater. Res.*, **43**(4), pp. 433–440.
- [22] Sohmura, T., 1988, "Improvement in Corrosion Resistance in Ti–Ni Shape Memory Alloy for Implant by Oxide Film Coating," Proceedings of the World Biomaterial Congress, Kyoto, Japan, p. 574.
- [23] Undisz, A., Schrempel, F., Wesch, W., and Rettenmayr, M., 2012, "Mechanism of Oxide Layer Growth During Annealing of NiTi," *J. Biomed. Mater. Res. A*, **100**(7), pp. 1743–1750.
- [24] Villermaux, F., Tabrizian, M., Yahia, L., Meunier, M., and Piron, D. L., 1997, "Excimer Laser Treatment of NiTi Shape Memory Alloy Biomaterials," *Appl. Surf. Sci.*, **109–110**, pp. 62–66.
- [25] Nishida, M., Wayman, C. M., and Honma, T., 1986, "Precipitation Processes in Near-Equiatomic TiNi Shape Memory Alloys," *Metall. Trans. A*, **17**(9), pp. 1505–1515.
- [26] Verdian, M. M., Raeissi, K., Salehi, M., and Sabooni, S., 2011, "Characterization and Corrosion Behavior of NiTi–Ti2Ni–Ni3Ti Multiphase Intermetallics Produced by Vacuum Sintering," *Vacuum*, **86**(1), pp. 91–95.
- [27] Landolt, D., 2002, "Introduction to Surface Reactions: Electrochemical Basis of Corrosion," *Corrosion Mechanisms in Theory and Practice*, P. Marcus, ed., Marcel Dekker, New York, pp. 1–17.
- [28] Jones, D. A., 1992, *Principles and Prevention of Corrosion*, MacMillan, New York.
- [29] Oldfield, J. W., 1988, *Galvanic Corrosion*, ASTM, Philadelphia, PA.
- [30] Deshpande, K. B., 2011, "Numerical Modeling of Micro-Galvanic Corrosion," *Electrochim. Acta*, **56**(4), pp. 1737–1745.
- [31] Chan, C. W., Man, H. C., and Yue, T. M., 2012, "Susceptibility to Stress Corrosion Cracking of NiTi Laser Weldment in Hanks' Solution," *Corros. Sci.*, **57**, pp. 260–269.

- [32] Yan, X.-J., and Yang, D.-Z., 2006, "Corrosion Resistance of a Laser Spot-Welded Joint of NiTi Wire in Simulated Human Body Fluids," *J. Biomed. Mater. Res. A*, **77**(1), pp. 97–102.
- [33] ASTM Standard F756-08 A., 2013, "Standard Practice for Assessment of Hemolytic Properties of Materials," ASTM International, West Conshohocken, PA, pp. 1–5.
- [34] ISO 10993-5 I., 2009, "Biological Evaluation of Medical Devices—Part 5: Tests for in Vitro Cytotoxicity," ISO/TC 194, Geneva, Switzerland.
- [35] ASTM Standard G5-14, 2014, "Standard Reference Test Method for Making Potentiodynamic Anodic Polarization Measurements," ASTM International, West Conshohocken, PA.
- [36] EPA Method 200.7, 1994, "Determination of Metals and Trace Elements in Water and Wastes by Inductively Coupled Plasma-Atomic Spectrometry," U.S. Environmental Protection Agency, Cincinnati, OH.
- [37] Visser, K. R., 1989, "Electric Conductivity of Stationary and Flowing Human Blood at Low Frequencies," IEEE Engineering in Medicine and Biology Society 11th Annual International Conference, pp. 1540–1542.
- [38] McMahon, R. E., Ma, J., Verkhovurov, S. V., Munoz-Pinto, D., Karaman, I., Rubitschek, F., Maier, H. J., and Hahn, M. S., 2012, "A Comparative Study of the Cytotoxicity and Corrosion Resistance of Nickel–Titanium and Titanium–Niobium Shape Memory Alloys," *Acta Biomater.*, **8**(7), pp. 2863–2870.
- [39] Satoh, G., 2013, *Modification and Integration of Shape Memory Alloys Through Thermal Treatments and Dissimilar Metal Joining*, Ph.D. thesis, Columbia University, New York.
- [40] Crone, W. C., Yahya, A. N., and Perepezko, J. H., 2001, "Influence of Grain Refinement on Superelasticity in NiTi," Proceedings of the SEM Annual Conference on Experimental Mechanics, Portland, OR, pp. 510–513.
- [41] Ralston, K. D., Birbilis, N., and Davies, C. H. J., 2010, "Revealing the Relationship Between Grain Size and Corrosion Rate of Metals," *Scr. Mater.*, **63**(12), pp. 1201–1204.
- [42] Shih, C. C., Lin, S. J., Chung, K. H., Chen, Y. L., and Su, Y. Y., 2000, "Increased Corrosion Resistance of Stent Materials by Converting Current Surface Film of Polycrystalline Oxide into Amorphous Oxide," *J. Biomed. Mater. Res.*, **52**(2), pp. 323–332.
- [43] Zhang, Y., Jiang, S., Liang, Y., and Hu, L., 2013, "Simulation of Dynamic Recrystallization of NiTi Shape Memory Alloy During Hot Compression Deformation Based on Cellular Automaton," *Comput. Mater. Sci.*, **71**, pp. 124–134.
- [44] Akgun, O. V., Urgan, M., and Kahir, A. F., 1995, "The Effect of Heat Treatment on Corrosion Behavior of Laser Surface Melted 304L Stainless Steel," *Mater. Sci. Eng. A*, **203**(1–2), pp. 324–331.
- [45] Prokofiev, E., Burow, J., Payton, E., Zarnetta, R., Frenzel, J., Gunderov, D. V., Valiev, R. Z., and Eggeler, G., 2010, "Suppression of Ni₄Ti₃ Precipitation by Grain Size Refinement in Ni-Rich NiTi Shape Memory Alloys," *Adv. Eng. Mater.*, **12**(8), pp. 747–753.